

## The Effect of SnO<sub>2</sub> Mixture on a PVA-Based Thick Film Relative Humidity Sensor

Goib Wiranto<sup>a,\*</sup>, Supeno Martadi<sup>b</sup>, M. Amin Sulthoni<sup>b</sup>, I Dewa Putu Hermida<sup>a</sup>, Yudi Y. Maulana<sup>a</sup>, Slamet Widodo<sup>a</sup>, Deni P. Kurniadi<sup>a</sup>, Pamungkas Daud<sup>a</sup>

<sup>a</sup> Smart Sensor Group, Indonesian Institute of Sciences, Jl. Sangkuriang, Bandung, 40135, Indonesia

<sup>b</sup> Bandung Institute of Technology, Jl. Ganesha, Bandung, Indonesia

Corresponding author: \*gwiranto@gmail.com

**Abstract**— In this research, thick film technology has been used to design and fabricate relative humidity sensors with Polyvinyl Alcohol (PVA) as the sensing layer. The design was optimized to produce an ideal geometry according to the limitations of thick film technology. The sensor fabrication process used screen printing techniques on Alumina (Al<sub>2</sub>O<sub>3</sub>) substrate with Silver (Ag) as the electrode material. SnO<sub>2</sub> was added to the PVA sensing layer with variations in the composition of 1:1 and 1:2. FTIR analysis showed that the addition of SnO<sub>2</sub> did not affect the structure of the PVA, which indicated that there was no chemical reaction between PVA and SnO<sub>2</sub>. The deposition of the sensing layer was carried out using spin coating method, and the fabricated sensors were then tested by varying 5 humidity points inside a chamber with a hygrometer as a reference. Based on the test results, it was found that the sensors showed responses to humidity variation in the form of changes in resistance values. When the humidity in the chamber increased, the sensor resistance value decreased. The addition of SnO<sub>2</sub> could reduce the relatively high resistance value of the PVA-based humidity sensor and also increase the sensor's time response to humidity variation. However, the humidity sensor's sensitivity decreased for the higher composition of SnO<sub>2</sub>. With this technique, a simple yet stable humidity sensor could be fabricated using thick-film technology with a wide range of potential applications.

**Keywords**— Relative humidity sensor; thick film technology; screen printing; spin coating; PVA; SnO<sub>2</sub>.

Manuscript received 5 Apr. 2021; revised 30 May 2021; accepted 7 Sep. 2021. Date of publication 30 Jun. 2022.  
IJASEIT is licensed under a Creative Commons Attribution-Share Alike 4.0 International License.



### I. INTRODUCTION

Nowadays, the measurement of moisture or humidity is an important aspect that has been applied in various fields such as food processing and storage [1], agriculture [2], pharmaceutical [3], biomedical [4], chemical [5], ecological [6], atmospheric weather condition [7], etc. Humidity can be defined as the amount of water vapor in the air, but the unit parameters for humidity can be expressed in various ways depending on the measurement techniques used. The most commonly used term is relative humidity (RH), or the ratio of the actual amount of moisture in the atmosphere to the amount of moisture that it can hold at the same given temperature and pressure [8]. Although various sensing approaches have been employed to measure the relative humidity in the environment for the past few years, study to search for better humidity sensors is still being conducted in large by many researchers.

Some of the most recent relative humidity sensors have employed new materials as moisture-sensitive layers. These

materials include porous ceramic oxides [9], [10], polymers [11], [12], and electrolytes [13], [14]. Ceramic oxides can be prepared by conventional or advanced processing, and their extensive use as humidity sensors is due to their hydrophilic nature, so water vapor can easily penetrate through the pore openings. For example, Ceramic Alumina (Al<sub>2</sub>O<sub>3</sub>) has demonstrated its ability to increase the sensor's sensitivity when used as a capacitive humidity sensor [15]. The porous structure of ceramic oxides also offers more active sites for sensing reactions, and thus nanocrystalline metal oxides such as zinc ferrite [16] and iron-titanium oxide [17] are promising candidates for humidity sensors. On the other hand, polymer materials have long been used as humidity sensors because of their availability in various forms. In dielectric type humidity sensors, polymer materials such as polyimide [18], polymethyl methacrylate (PMMA) [19], and polyvinyl alcohol (PVA) [20], have been used to bind water molecules between two electrodes such that humidity measurement can

be performed through changes in the dielectric constant of the polymer materials.

Another important development in humidity sensor fabrication is the use of thick film technology, where sensor's sensitive layers can be screen printed on a ceramic (usually alumina) and flexible substrates [21], [22]. Screen printing is done by squeezing a paste material through a (stainless-steel) mesh with predefined patterns. Various materials can be screen printed for sensor application, including polymers, ceramics, metal, and semiconductors [23]. This technique can produce fine line paths in the range of a few micrometers, which is suitable for device miniaturization. With the main advantage of being low in manufacturing cost, many humidity sensors have been fabricated using thick-film technology [24,25].

This research has focused on designing and fabricating PVA-based relative humidity sensors using thick-film technology. The sensitive layer was made from PVA mixed with SnO<sub>2</sub> metal oxide, and the humidity sensor's operation was based on changes in resistance values of the PVA-SnO<sub>2</sub> sensitive layer. The design, fabrication, and the effect of SnO<sub>2</sub> addition to the PVA-based humidity sensor will be presented in this paper.

## II. MATERIALS AND METHOD

### A. Sensor Design

The structure of the humidity sensor consisted of an alumina (Al<sub>2</sub>O<sub>3</sub>) substrate, an interdigital silver (Ag) electrode, and a PVA based sensitive layer, as can be seen in Figure 1. The sensor layout has been designed in a 10 x 25 mm alumina substrate. The line width of the silver electrode and the spacing between the electrode tracks were 0.5 mm. The layout aimed to produce optimal geometry according to the capability limit of thick film technology and prevent failures during sensor fabrication. The design of each layer was then transferred to a stainless-steel mesh using a photolithographic process.

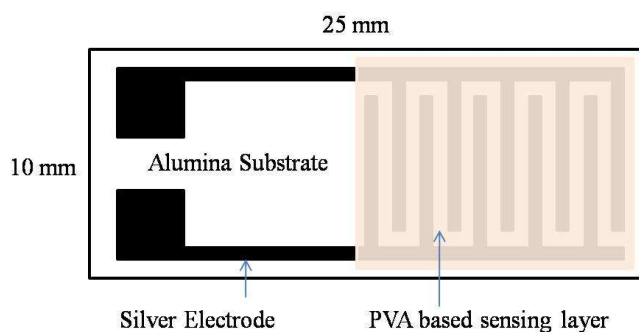


Fig. 1 Structure of the humidity sensor device

### B. Sensor Fabrication

Fabrication of the sensor device was started by screen printing the interdigital electrode using silver paste, followed by drying and firing process at high temperature to remove any organic solvent from the printed electrode tracks. Since the alumina substrate was 5 x 5 cm, 10 devices could be printed simultaneously. Each device was then cut manually from the substrate using a diamond cutter.

The next step of fabrication of the humidity sensor was deposition of the PVA based sensing layer. Prior to the

deposition, PVA as the starting material was mixed with SnO<sub>2</sub> powder with ratio of 1:1 and 1:2 by weight. Distilled water was added to each mixture and the resulting composition was mixed using magnetic stirrer for 60 min at a temperature of 90 °C. To maintain the polymeric structure of the mixture, an APS (ammonium peroxydisulfate) was added upon cooling. The addition of APS also aimed to reduce swelling and create a strong PVA matrix network [26]. Finally, the sensing layer deposition was carried out using the pin coating method for 10 seconds at a speed of 2000 rpm. The device was then dried in the oven at 105 °C for 25 min.

## III. RESULTS AND DISCUSSION

### A. Sensing Layer Structural Characteristics

To determine the structural characteristics of the sensing layer, an FTIR (Fourier Transform Infra-Red) test was performed. Based on the test results, as shown in Figure 2, it is obvious that the peaks representing the O-H group type (phenol compounds or hydrogen bond) are seen in the frequency area of 3200 – 3600 cm<sup>-1</sup>. The peaks in the frequency range of 2800 – 3000 cm<sup>-1</sup> are C-H group type alkane compounds, and the peaks at the frequency area of 1000 – 1200 cm<sup>-1</sup> are C-O group compounds of alcohol and ether carboxylic acid or ester. Based on the FTIR results, it can be said that a sensing layer is an alcohol group. The graph also shows no significant difference between the samples, which indicated no chemical reaction between PVA, APS, and SnO<sub>2</sub>.

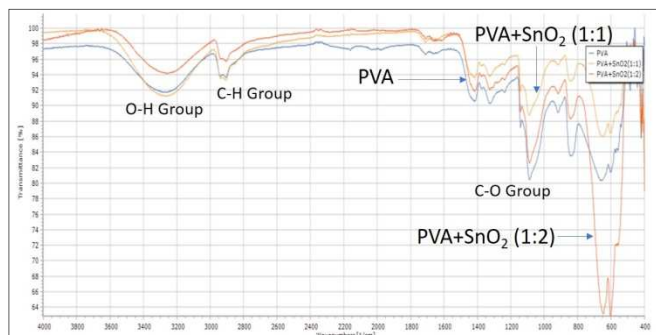


Fig. 2 FTIR test results of the PVA based sensitive layer

### B. Morphology and Composition of The Sensing Layer

SEM (Scanning Electron Microscopy) and EDS (Energy Dispersive X-ray Spectroscopy) characterization were performed to determine the morphology and composition of the sensing layer. Based on the SEM test results for the three sensing layers using a magnification of 5000x, PVA is in the form of large irregular granules, as shown in Figure 3a. While in Figure 3b, PVA+SnO<sub>2</sub> (1:1) shows that SnO<sub>2</sub> is in the form of small white granules that are scattered over the surface, a slightly different from Figure 3c where PVA+SnO<sub>2</sub> (1:2) shows that the amount of SnO<sub>2</sub> granules that are more widely distributed on the surface.

The fact that the morphology of the PVA has changed when mixed with SnO<sub>2</sub> was confirmed by the EDS test results. Such change was possible to occur during the process of making the sensing layer, where SnO<sub>2</sub> eroded PVA due to differences in mass and size of the two materials. Figure 4a shows the EDS result for PVA sensing layer, and Figure 4a and 4b are

the results of PVA+SnO<sub>2</sub>. The change in concentration of Sn is greater for the higher mixture composition; that is, in PVA+SnO<sub>2</sub> (1:2), the concentration of Sn is greater than O, and almost twice the concentration of C. Table 1 shows the detailed concentration of each component in the PVA+SnO<sub>2</sub> mixture.

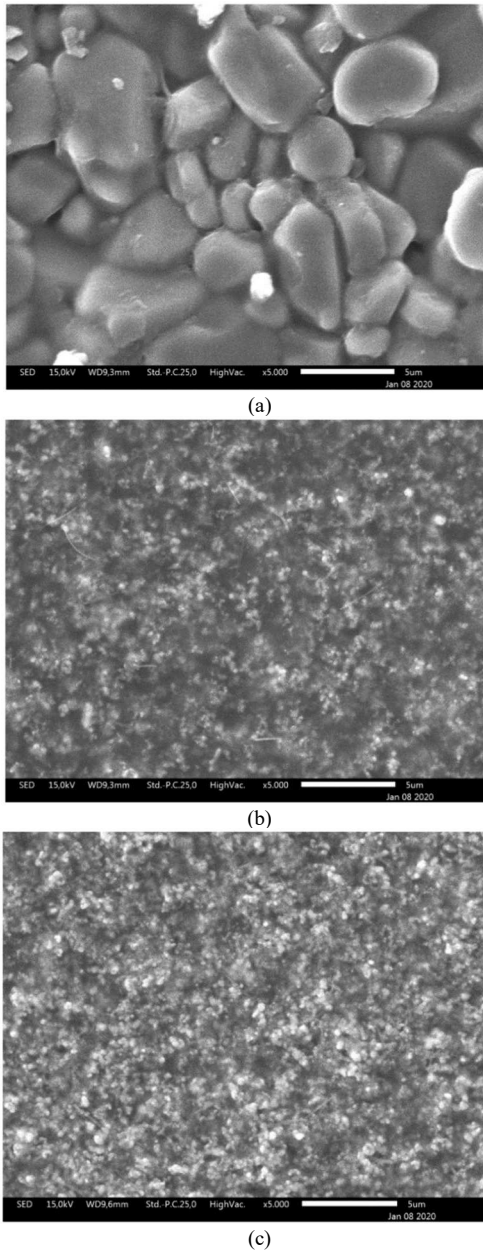


Fig. 3 SEM images of the sensing layer (a). PVA, (b). PVA+SnO<sub>2</sub> (1:1), and (c). PVA+SnO<sub>2</sub> (1:2)

### C. Effects of SnO<sub>2</sub> Concentration on Resistance

The resistivity test has been conducted according to the schematic shown in Figure 5. This test was carried out to see the effect of a mixture of SnO<sub>2</sub> concentrations on PVA by comparing the sensor resistance values. As such, the sensor resistance measurement was done at five humidity points and averaged the resulting values. The sample was given a 5 V supply voltage and a maximum current of 20 mA at a temperature of 25°C. The measurement settings were done from the Kickstartfl-HRMA application (Keithly).

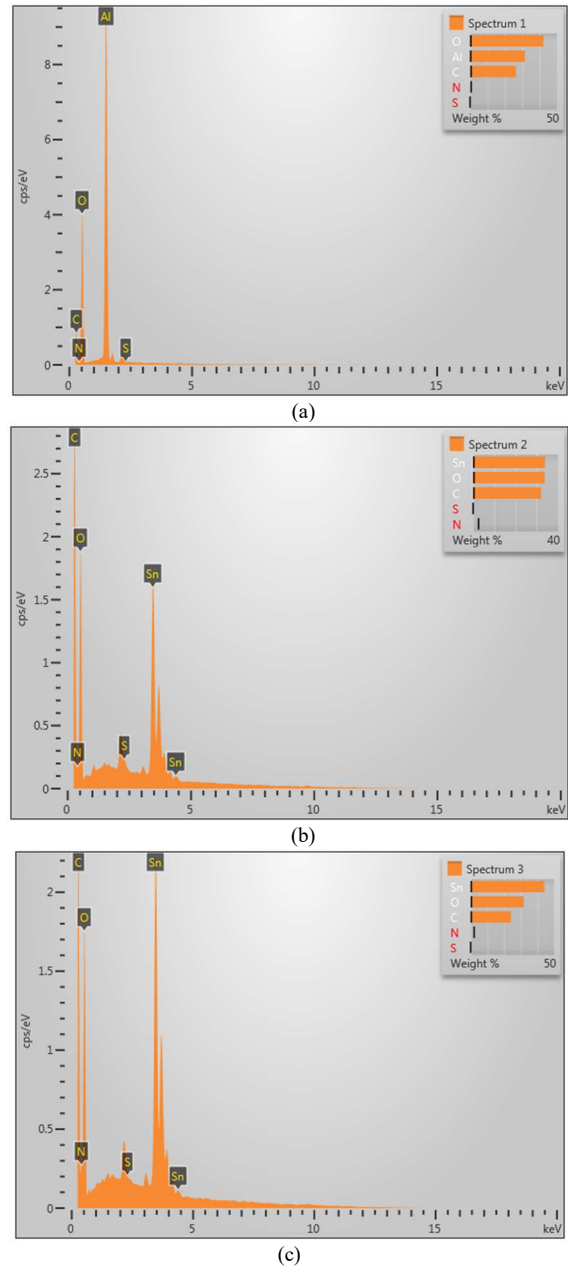


Fig. 4 EDS test results of the sensing layer (a). PVA, (b). PVA+SnO<sub>2</sub> (1:1), and (c). PVA+SnO<sub>2</sub> (1:2)

TABLE I  
ELEMENT CONCENTRATION OF THE SENSING LAYER

Element	Wt%		
	PVA	PVA+SnO <sub>2</sub> (1:1)	PVA+SnO <sub>2</sub> (1:2)
C	26.33	32.03	24.13
O	42.17	33.76	31.80
Sn	-	33.90	44.07

Table II shows the results of testing the effect of SnO<sub>2</sub> concentration on sensor resistance. The test shows the resistance of the three sensors decreased from 108 Ω at 16% RH to 104 Ω at 85% RH, as shown in Figure 6. Based on the testing, the fabricated relative humidity sensor responds to humidity in the form of changes in resistance. It was also found that the concentration of the SnO<sub>2</sub> mixture in the PVA as the sensing layer affects the sensor resistance, where the higher the SnO<sub>2</sub> concentration, the lower the sensor resistance.

It can be seen from the graph that the sensor resistance with PVA+SnO<sub>2</sub> (1:2) as the sensing layer shows a lower resistance value.

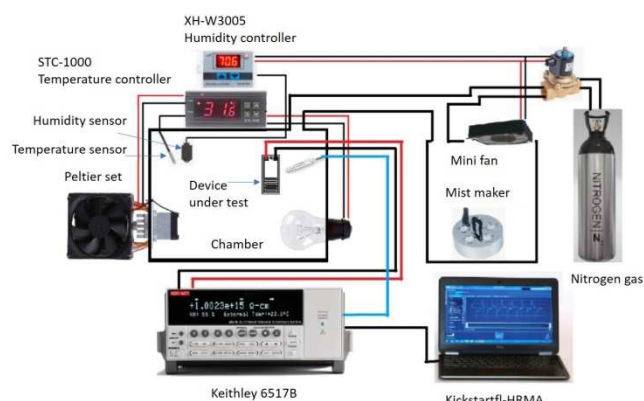


Fig. 5 Experimental setup for the measurement of relative humidity sensors

TABLE II  
RESISTANCE VALUES OF PVA BASED SENSING LAYER

RH (%)	Resistance ( $\Omega$ )		
	PVA	PVA+SnO <sub>2</sub> (1:1)	PVA+SnO <sub>2</sub> (1:2)
16	8.08E+08	5.91E+08	4.83E+08
44	3.00E+08	2.27E+08	2.65E+07
57	4.08E+06	3.00E+06	1.20E+06
76	1.27E+05	7.09E+04	2.35E+04
85	5.26E+04	5.23E+04	1.30E+04

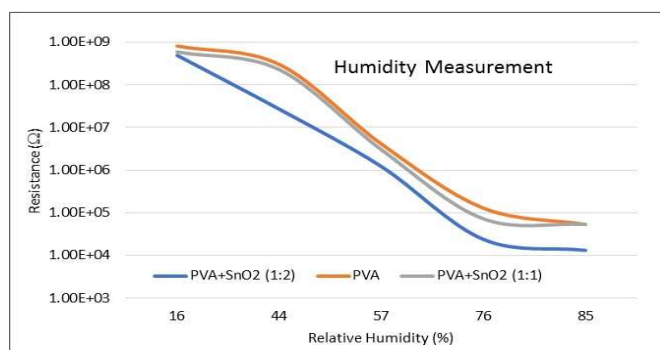


Fig. 6 The effect of SnO<sub>2</sub> concentration on-resistance of the sensing layer

Additional properties of SnO<sub>2</sub> can be explained by the use of other similar metal oxides such as TiO<sub>2</sub> [27]. Adsorption of water molecules begins with forming a chemisorbed layer, where SnO<sub>2</sub> forms a bond with OH ion. The hydroxyl group will then bond with the adsorbed H<sub>2</sub>O to form the first physically adsorbed layer. Water molecules cannot move freely in this layer because an electric force binds them with two hydroxyl groups. The H<sup>+</sup> proton can only move from hydroxyl groups to water molecules to form H<sub>3</sub>O<sup>+</sup>. The water vapor adsorption process continues to form a second physisorbed layer where H<sup>+</sup> ions hopping can take place between water vapor molecules. This modeling shows that the PVA-SnO<sub>2</sub>-based sensing layer has a high conductivity value when adsorption occurs with a water molecule.

#### D. Sensor Sensitivity

Based on the data in Table II, the sensitivity of the sensing layers at various humidity levels can be calculated. Simply by

taking the average values between the highest and the lowest humidity levels. Figure 7 shows the calculated sensitivity values for the three sensing layers. As can be seen, the sensor with PVA+SnO<sub>2</sub> (1:2) as the sensing layer has a lower sensitivity ( $\Omega$  /% RH) compared to the other two sensors. In other words, SnO<sub>2</sub> reduces sensor sensitivity, and thus sensors with PVA+SnO<sub>2</sub> (1:2) as the sensing layer are the least sensitive sensors. This is possible because the hopping process of H<sup>+</sup> ions on metal oxide SnO<sub>2</sub> occurs after the second physisorbed layer is formed.

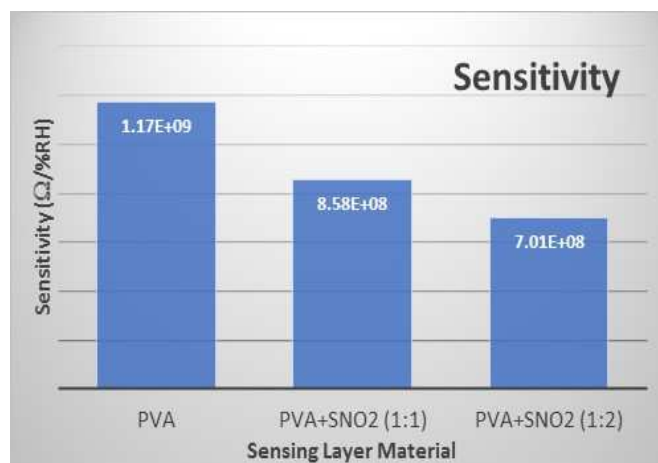


Fig. 7 The sensitivity of the sensing layers

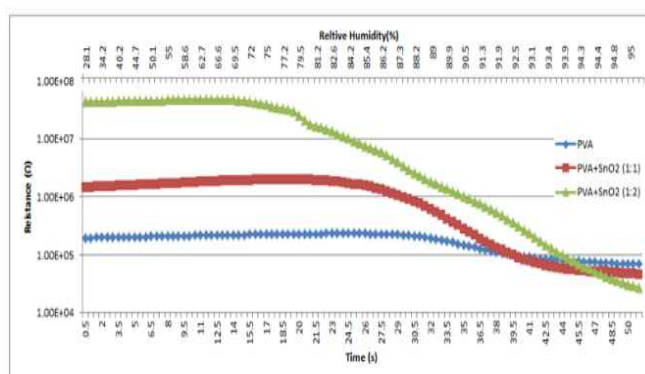


Fig. 8 Response time of the humidity sensors

#### E. Response Time

This test aimed to compare each sensor's response to a sudden change in humidity condition. As such, the humidity chamber (RH) was initially set to the minimum value, and the sensor was then undergoing an abrupt humidity change within 0.5 second to the maximum humidity value. To get more detailed and accurate results, changes in the humidity chamber were done using Kickstartfl-HRMA application.

The results of this test are shown in Figure 8. It was found that the sensor with PVA+SnO<sub>2</sub> (1:2) as the sensing layer responded more rapidly to sudden changes in humidity (RH) when compared to the other two sensors. PVA+SnO<sub>2</sub> (1:2) responded by decreasing resistance at 12.5 seconds, PVA+SnO<sub>2</sub> (1:1) responded at 20.5 seconds, and PVA decreased resistance at 26 seconds. This is similar to testing the PVA response to humidity, which is possible because in PVA+SnO<sub>2</sub> the transfer of H<sup>+</sup> ions occur not only in PVA but also in the second physisorbed layer of SnO<sub>2</sub> produced.

## F. Circuit Modeling

From testing the sensor's response to humidity, the sensor conductivity can be modeled by a series circuit, where the circuit model consists of SnO<sub>2</sub> resistance supplied with PVA resistance, as shown in Figure 9. Changes in sensor resistance depend on changes in PVA and SnO<sub>2</sub> resistance.

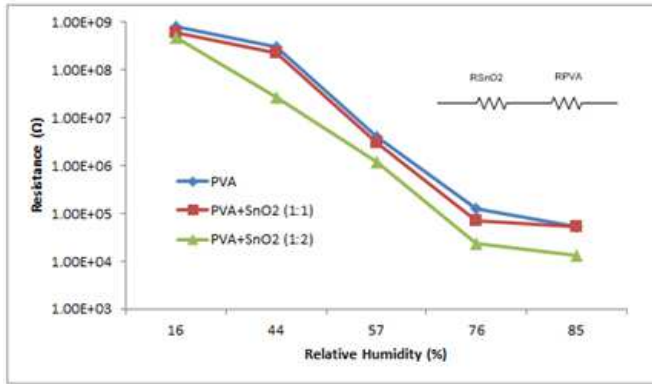


Fig. 9 Circuit modeling of the humidity sensors

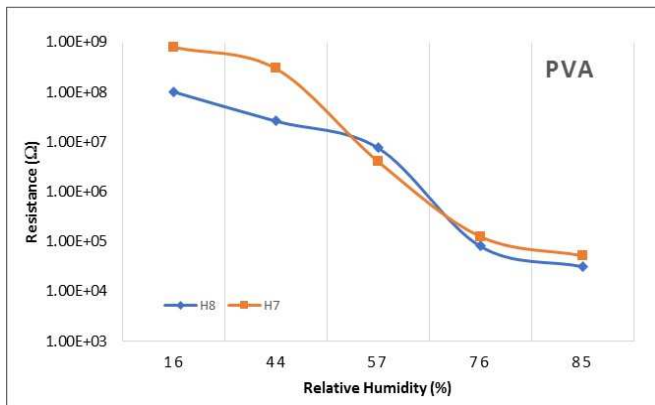


Fig. 10 Comparison of sensor resistance with PVA as the sensing layer

## G. Effect of Differences in The Number of Electrodes on Resistance

In this test, the resistance was compared between the designs with five electrode pairs (H7) and seven electrode pairs (H8). The tests were carried out on three samples of the H8 design sensors, and the results were then compared with the results of the H7 design tests that had been carried out previously. The test results of the H7 and H8 designs with PVA as the sensing layer are shown in Figure 10. The resistance value of the H8 design sensor has four values lower than the H7 design.

The comparison results of design H7 and H8 sensor resistance with PVA+SnO<sub>2</sub> (1:1) as the sensing layer are shown in Figure 11, while the comparison results of H7 and H8 design sensor resistance with PVA+SnO<sub>2</sub> (1:2) as the sensing layer are shown in Figure 12. Based on the test results, differences in sensor design have caused differences in sensor resistance. In general, the more electrode legs from the sensor, the lower the sensor resistance.

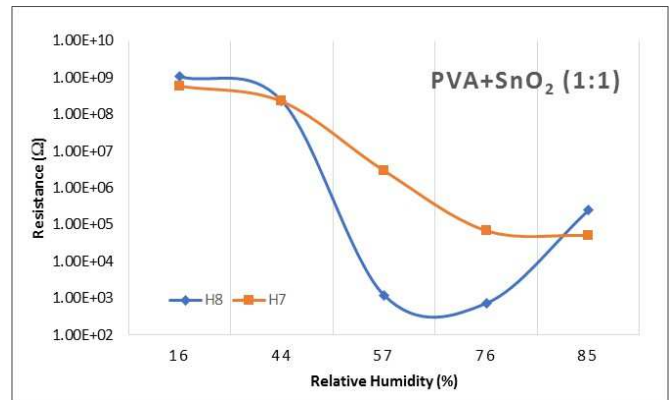


Fig. 11 Comparison of sensor resistance with PVA+SnO<sub>2</sub> (1:1) as the sensing layer

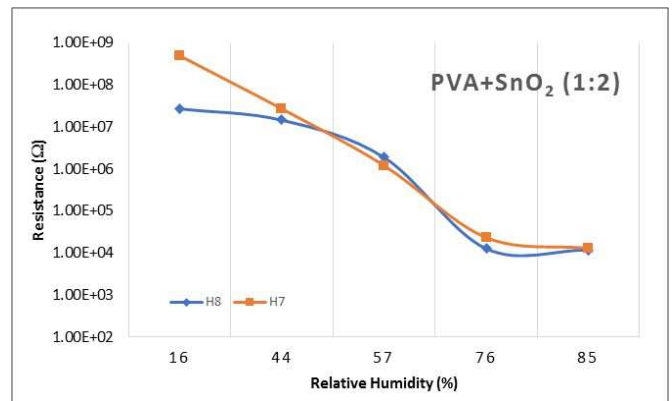


Fig. 12 Comparison of sensor resistance with PVA+SnO<sub>2</sub> (1:2) as the sensing layer

## IV. CONCLUSION

PVA-based relative humidity sensors have been successfully manufactured on alumina substrates using thick-film technology with dimensions of 25 mm x 10 mm. The addition of APS (ammonium peroxydisulfate) (NH<sub>4</sub>)<sub>2</sub>S<sub>2</sub>O<sub>8</sub>, and SnO<sub>2</sub> did not change the structure of the PVA, as evidenced from the graph of the FTIR test results that there were no significant differences between the three samples. This indicates no chemical reaction between PVA, APS, and SnO<sub>2</sub>.

The concentration of SnO<sub>2</sub> mixture in the PVA as the sensing layer affects the value of the resistance and response time of the sensor. The higher the concentration of SnO<sub>2</sub>, the lower the sensor resistance value, and the faster the response time to changes in humidity. The increase in conductivity and response time of PVA+SnO<sub>2</sub> occurred due to the displacement of H<sup>+</sup> ions to the PVA and in the physisorbed layer produced by SnO<sub>2</sub>. The higher the concentration of SnO<sub>2</sub>, the lower the sensor's sensitivity. This occurs because of the hopping phenomena of the H<sup>+</sup> ions on metal oxide after the second physisorbed layer is formed. The more the number of sensor electrode legs, the lower the sensor resistance value because the sensor resistance is paralleled by the number of electrode legs and the sensing area.

## ACKNOWLEDGMENT

We thank LPTB (Research Unit for Clean Technology) LIPI for facilitating the characterization using XRD and EDS.

## REFERENCES

- [1] A. Popa *et al.*, “An intelligent IoT-based food quality monitoring approach using low-cost sensors,” *Symmetry*, vol. 11, no. 3, 2019, doi: 10.3390/sym11030374.
- [2] J. Rodríguez-Robles, Á. Martín, S. Martín, J. A. Ruipérez-Valiente, and M. Castro, “Autonomous sensor network for rural agriculture environments, low cost, and energy self-charge,” *Sustain.*, vol. 12, no. 15, 2020, doi: 10.3390/SU12155913.
- [3] G. Wang *et al.*, “Fast-response humidity sensor based on laser printing for respiration monitoring,” *RSC Adv.*, vol. 10, no. 15, pp. 8910–8916, 2020, doi: 10.1039/c9ra10409g.
- [4] C. He *et al.*, “Real-time humidity measurement during sports activity using optical fibre sensing,” *Sensors*, vol. 20, no. 7, pp. 1–12, 2020, doi: 10.3390/s20071904.
- [5] S. F. Shaikh *et al.*, “Continuous hydrothermal flow-inspired synthesis and ultra-fast ammonia and humidity room-temperature sensor activities of WO<sub>3</sub> nanobricks,” *Mater. Res. Express*, vol. 7, no. 1, 2020, doi: 10.1088/2053-1591/ab67fc.
- [6] A. Enjin, “Humidity sensing in insects — from ecology to neural processing,” *Curr. Opin. Insect Sci.*, vol. 24, no. October, pp. 1–6, 2017, doi: 10.1016/j.cois.2017.08.004.
- [7] R. Arun Chakravarthy, M. Bhuvanewari, and M. Arun, “IoT based environmental weather monitoring and farm information tracking system,” *J. Crit. Rev.*, vol. 7, no. 7, pp. 307–310, 2020, doi: 10.31838/jcr.07.07.49.
- [8] H. Farahani, R. Wagiran, and M. N. Hamidon, “Humidity sensors principle, mechanism, and fabrication technologies: A comprehensive review,” *Sensors*, vol. 14, no. 5, pp. 7881 – 7939, 2014, doi: 10.3390/s140507881.
- [9] G. B. Crochemore, A. R. P. Ito, C. A. Goulart, and D. P. F. de Souza, “Identification of humidity sensing mechanism in MgAl<sub>2</sub>O<sub>4</sub> by impedance spectroscopy as function of relative humidity,” *Mater. Res.*, vol. 21, no. 4, 2018, doi: 10.1590/1980-5373-mr-2017-0729.
- [10] M. V. Nikolic *et al.*, “Structural, morphological and textural properties of iron manganite (FeMnO<sub>3</sub>) thick films applied for humidity sensing,” *Mater. Sci. Eng. B Solid-State Mater. Adv. Technol.*, vol. 257, no. April, p. 114547, 2020, doi: 10.1016/j.mseb.2020.114547.
- [11] J. Majewski, “Low humidity characteristics of polymer-based capacitive humidity sensors,” *Metrol. Meas. Syst.*, vol. 24, no. 4, pp. 607–616, 2017, doi: 10.1515/mms-2017-0048.
- [12] B. Deshkulkarni, L. R. Viannie, S. V. Ganachari, N. R. Banapurmath, and A. Shettar, “Humidity sensing using polyaniline/polyvinyl alcohol nanocomposite blend,” *IOP Conf. Ser. Mater. Sci. Eng.*, vol. 376, no. 1, 2018, doi: 10.1088/1757-899X/376/1/012063.
- [13] Muhammad Tariq Saeed Chani *et al.*, “Humidity sensor based on orange dye and graphene solid electrolyte cells,” *Russ. J. Electrochem.*, vol. 55, no. 12, pp. 1391–1396, 2019, doi: 10.1134/S1023193519120036.
- [14] T. Li *et al.*, “Porous ionic membrane based flexible humidity sensor and its multifunctional applications,” *Adv. Sci.*, vol. 4, no. 5, 2017, doi: 10.1002/advs.201600404.
- [15] A. Salamat and T. Islam, “Fabrication of an anodized porous alumina relative humidity sensor with improved sensitivity,” *Instrum. Sci. Technol.*, vol. 48, no. 2, pp. 128–145, 2020, doi: 10.1080/10739149.2019.1662803.
- [16] M. V. Nikolic *et al.*, “Investigation of ZnFe<sub>2</sub>O<sub>4</sub> spinel ferrite nanocrystalline screen-printed thick films for application in humidity sensing,” *Int. J. Appl. Ceram. Technol.*, vol. 16, no. 3, pp. 981–993, 2019, doi: 10.1111/ijac.13190.
- [17] M. V. Nikolic *et al.*, “Humidity sensing properties of nanocrystalline pseudobrookite (Fe<sub>2</sub>TiO<sub>5</sub>) based thick films,” *Sensors Actuators, B Chem.*, vol. 277, pp. 654–664, 2018, doi: 10.1016/j.snb.2018.09.063.
- [18] H. Liu *et al.*, “Humidity sensors with shielding electrode under interdigitated electrode,” *Sensors*, vol. 19, no. 3, 2019, doi: 10.3390/s19030659.
- [19] Z. Harith, H. Adnan Abdullah Zain, M. Batumalay, and S. Wadi Harun, “A study on relative humidity sensors using PVA and PMMA coating,” *J. Phys. Conf. Ser.*, vol. 1371, no. 1, 2019, doi: 10.1088/1742-6596/1371/1/012027.
- [20] S. Automation, G. R. Biswal, S. Member, P. Mohanty, and K. J. Akram, “Design and fabrication of an inexpensive capacitive humidity sensor for smart sub-station automation,” *IEEE Sens. J.*, vol. 20, no. 12, pp. 6215–6223, 2020.
- [21] V. S. Turkani *et al.*, “A highly sensitive printed humidity sensor based on a functionalized MWCNT/HEC composite for flexible electronics application,” *Nanoscale Adv.*, vol. 1, no. 6, pp. 2311–2322, 2019, doi: 10.1039/c9na00179d.
- [22] A. Rivadeneyra *et al.*, “Carbon dots as sensing layer for printed humidity and temperature sensors,” *Nanomaterials*, vol. 10, no. 12, p. 2446, 2020, doi: 10.3390/nano10122446.
- [23] D. Antuña-Jiménez, M. B. González-García, D. Hernández-Santos, and P. Fanjul-Bolado, “Screen-printed electrodes modified with metal nanoparticles for small molecule sensing,” *Biosensors*, vol. 10, no. 2, pp. 1–22, 2020, doi: 10.3390/bios10020009.
- [24] M. Awais, M. U. Khan, A. Hassan, J. Bae, and T. E. Chattha, “Printable highly stable and superfast humidity sensor based on two dimensional molybdenum diselenide,” *Sci. Rep.*, vol. 10, no. 1, pp. 1–13, 2020, doi: 10.1038/s41598-020-62397-x.
- [25] J. R. McGhee, J. S. Sagu, D. J. Southee, P. S. A. Evans, and K. G. Upul Wijayantha, “Printed, fully metal oxide, capacitive humidity sensors using conductive indium tin oxide inks,” *ACS Appl. Electron. Mater.*, vol. 2, no. 11, pp. 3593–3600, 2020, doi: 10.1021/acsaelm.0c00660.
- [26] T. Yonehara and H. Goto, “Synthesis of polyaniline/scarlet 3R as a conductive polymer,” *Polymers*, vol. 12, no. 3, 2020, doi: 10.3390/polym12030579.
- [27] M. Vishwas, K. N. Rao, D. N. Priya, A. M. Raichur, R. P. S. Chakradhar, and K. Venkateswarlu, “Effect of TiO<sub>2</sub> nano-particles on optical, electrical and mechanical properties of poly (vinyl alcohol) films,” *Procedia Mater. Sci.*, vol. 5, pp. 847–854, 2014, doi: 10.1016/j.mspro.2014.07.370.